Effect of zirconium and vanadium on electro-spark deposited AlNiCrTi high-entropy alloy coatings: microstructure and wear behavior

E. Kh. Ri, *Doctor of Technical Sciences, Professor, CEO of the Higher School of Industrial Engineering of the Polytechnic Institute[1], erikri999@mail.ru*
M. A. Ermakov*, Candidate of Technical Sciences, Associate Professor of the Higher School of Industrial Engineering of the Polytechnic Institute[1], ermakovma@yandex.ru*
E. D. Kim*, Candidate of Technical Sciences, Assistant Professor of the Higher School of Industrial Engineering of the Polytechnic Institute[1], jenya_1992g@mail.ru*
K. V. Doroshenko*, Post-Graduate Student of the Higher School of Industrial Engineering of the Polytechnic Institute[1], rbhbkk1212@yandex.ru*

[1]Pacific National University (Khabarovsk, Russia).

This paper presents a comprehensive study of the influence of alloying elements – zirconium and vanadium – in high-entropy anode alloys of the Al – Ni – Cr – Ti – V_x – Zr_{1-x} system on the microstructure, phase composition, mechanical, and tribological properties of electro-spark deposition (ESD) coatings applied to C45 steel.
Anode alloys with varying contents of zirconium (from 4.46 to 11.17 wt.%) and vanadium (from 17.84 to 5.36 wt.%) were produced by self-propagating high-temperature synthesis (SHS). The coatings were formed using an "Elitron-21" ESD unit in an argon atmosphere. Analysis was carried out using scanning electron microscopy (SEM), *X*-ray diffraction (XRD), microhardness measurements, and abrasive wear testing according to the "ball-on-plane" scheme.
It was found that all of the alloys under investigation form highly adherent coatings on the steel substrate that are free of longitudinal cracks. The coating microstructure is characterized by columnar crystallites. The main phase in both the coatings and the anode alloys is a solid solution based on the system's elements, alloyed with zirconium and vanadium. The results showed a direct correlation between the zirconium content and the operational properties of the coatings. The maximum values of microhardness (1088 HV) and wear resistance (5 times higher than that of untreated C45 steel) were achieved using an anode alloy with a zirconium content of 10.4 wt.% (Alloy 4).
Transverse microcracks were observed in the coatings, caused by deposition stresses and the brittleness of intermetallic phases. An interesting finding was the identification of two-layer areas, free from cracks, in which the lower barrier layer of crystallites was significantly enriched with iron (up to 73 at.%) that had diffused from the substrate. This indicates the promise of further investigation into the formation mechanism of such iron-saturated layers for the targeted control of the structure and reduction of brittleness in ESD coatings. This research direction will allow for further optimization of their properties for application under conditions of intense abrasive wear.

Key words: Electro-spark deposition (ESD), wear-resistant coatings, high-entropy alloys (HEA), zirconium, vanadium, microhardness, microstructure, abrasive wear.

DOI: 10.17580/nfm.2026.01.06

Introduction

Wear-resistant coatings offer a technically and economically viable solution for enhancing the strength and restoring the surfaces of machine components subjected to severe wear. To prevent or delay the onset of surface damage, various conventional surface engineering techniques are employed, such as Physical Vapor Deposition (PVD), Chemical Vapor Deposition (CVD), electroplating, and thermal diffusion (e.g., TD) processes. While these methods are widely used to improve surface hardness, wear resistance, and corrosion performance [1], they possess inherent limitations, including high capital costs, environmental concerns, and lengthy processing times.

Electro-spark deposition (ESD) has emerged as a promising alternative, offering advantages in cost-effectiveness, operational simplicity, and environmental friendliness [2–8]. This technique enables the application of high-quality, durable coatings onto metallic components of virtually any size or geometry.

Despite its benefits, ESD faces challenges, notably an insufficient understanding of coating microstructure evolution and a limited selection of optimized anode materials [9–11]. To address these limitations, high-entropy alloys (HEAs) present a compelling candidate material system for ESD coatings. HEAs are known for their tunable properties and exceptional performance under severe conditions, attributed to core effects such as high

configurational entropy, the "cocktail" effect, severe lattice distortion, and sluggish diffusion [12]. Recent studies have demonstrated that HEAs can surpass conventional alloys, exhibiting high strength [13], exceptional corrosion resistance [14], and superior wear resistance [15], which underscores their potential for demanding structural applications [16–18]. Their notable combination of strength and toughness [19, 20] is particularly advantageous.

Furthermore, ESD, as noted by Jihui Yan et al. [21], provides a low-cost, precise coating method that minimizes thermal damage to the substrate and ensures strong adhesion. Literature also highlights that ESD-fabricated AlCrFeCoNi coatings exhibit excellent wear resistance and hardness, making them ideal for wear-protection applications without the need for post-processing [22].

This work investigates the influence of zirconium and vanadium content in HEA anode materials on the microstructure and wear resistance of both the bulk alloys and the resulting ESD coatings. Zirconium was selected due to its well-known ability to form thermally stable intermetallics and oxides, which contribute to dispersion strengthening and enhance high-temperature stability. Vanadium was introduced as strong carbide and nitride former, as well as an element that increases hardness and wear resistance through solid solution strengthening. The combination of these elements within the Al – Ni – Cr – Ti system aims to synergistically improve the mechanical and tribological properties of both the anode alloys and the resulting coatings.

Materials and experimental methods

Coatings were deposited on Grade C45 steel samples. The choice of this steel is justified by its common use for manufacturing machine components and parts. The coating is designed to serve as a wear-resistant contact surface under dry friction conditions.

The coatings were applied using high-entropy anode alloys fabricated via liquid-phase Self-propagating High-temperature Synthesis (SHS). The initial charge mixture consisted of metal oxides (NiO (99.5 wt.%, TU 6-09-3642–74, Grade 10-2), TiO_2 (99.9 wt.%, TU 6-09-2166–77, Pure Grade), Cr_2O_3 (99.9 wt.%, GOST 2912–79, Analytical Reagent), V_2O_5 (99 wt.%, TU 6-09-4093–75, Analytical Reagent), ZrO_2 (99.9 wt.%, TU 6-09-4709–79, Reagent Grade)) and technical-grade calcium fluoride (CaF_2). Aluminum powder (Grade PA-4) with an average particle size of 50 μm was used as a reducing agent.

The coatings were deposited using an "Elitron-21" electro-spark treatment unit. A standard vibrating tool holder operating at a frequency of 100 Hz was employed as the anode holder. To prevent oxidation during the ESD process, an argon purge was maintained at a flow rate of approximately 3.5 L/min.

The quality of the resulting coatings (presence and quantity of oxides and microcracks) was evaluated visually using a "Labomet M" metallographic microscope. The elemental composition of structural components was analyzed using a Hitachi "SU-70" LS10 Scanning Electron Microscope (SEM) equipped with a Thermo Fisher Scientific "UltraDry" energy-dispersive *X*-ray spectroscopy (EDS) detector. The phase composition of the anode materials and coatings was determined by *X*-ray diffraction (XRD) on a DRON-7 diffractometer (Cu-$K\alpha$ radiation), using qualitative analysis software and PDF database standards from PD Win.

The microhardness of the cast alloys and the resulting coatings was measured on a Shimadzu "HMV-G" microhardness tester. Additionally, to assess the micro-brittleness of the coatings, indentation imprints (load 150–200 g) obtained on polished cross-sections of the coatings were examined using the same Shimadzu "HMV-G" instrument, following an established methodology and rating scale [23].

Wear resistance tests were conducted on a CALOTEST unit (CSM Instruments) using a "ball-on-plane" configuration under abrasive wear conditions. A normal load of 0.24 N and a constant sliding speed of 0.61 m/s were applied. A 20 mm diameter ball made of VK6 (WC-6%Co) carbide served as the abrasive counter-body. A suspension containing Al_2O_3 powder (5 g) and RENEP CGLP 68 oil (50 ml) was supplied to the contact zone. Wear resistance was measured gravimetrically using a "Gosmetr VL-210" electronic balance.

Results and discussion

Table 1 presents the elemental composition of the as-cast alloys (1–5) used as anode materials for coating deposition. The primary compositional differences among the alloys lie in the zirconium and vanadium content, with their concentrations increasing from 5 to 18 wt.%.

Metallographic analysis of the anode alloys was performed on cross-sectional, ground samples of the obtained ingots. The macrostructure of the metallic ingots exhibits fine pores (up to 0.3×10^{-4} m), occasionally filled with slag inclusions. The porosity is of a scattered nature, primarily located in the central part of the ingots. The microstructure of the alloys (1–5) does not differ significantly from one another, exhibiting a uniform and fine-grained structure **(Fig. 1,** *a*, *b***)**, which is attributed to their similar elemental composition and identical melting conditions.

Fig. 1, *e* presents the *X*-ray diffraction (XRD) patterns of the synthesized alloys. The discrepancies in the intensi-

Table 1
Elemental composition of the fabricated anode alloys

Alloy	Content of elements in the alloy, wt. %					
	Al	Ti	V	Cr	Ni	Zr
1	25.55	16.72	17.84	18.88	16.55	4.46
2	25.90	16.38	13.40	21.57	17.14	5.62
3	26.83	15.84	10.15	20.52	18.73	7.92
4	27.11	15.01	7.52	21.02	18.93	10.40
5	25.70	17.72	5.36	20.86	19.19	11.17

ty and position of the reflections between the experimental XRD patterns and the standard PD Win database files are attributed to the varying crystallographic orientation of the crystals **(Fig. 1, *a–e*)** in local areas of the samples. Furthermore, the peak shifts in the diffraction patterns are caused by the presence of complex alloying elements and fine pores within the alloys.

Based on the analysis of the obtained results, it is established that the primary phase in the anode alloys is a solid solution based on Al – Ni – Ti – Cr, alloyed with Zr and V. The phase composition of the matrix in the synthesized alloys is corroborated by the microhardness analysis results (**Table 2**), which are consistent with findings from other studies.

The presence of scattered porosity and oxide inclusions in the central part of the ingots, characteristic of the SHS process, did not critically affect the homogeneity and adhesion of the resulting ESD coatings. This is explained by the localized nature of melting and material transfer during electro-spark deposition, where the surface layer of the anode plays the primary role.

Some variations in the composition of alloys 1–5 **(Fig. 1, *a–e*)** are recorded in **Table 2**. The structure of the synthesized anode alloys consists of grains of an Al, V, Ti, Cr-based solid solution, alloyed with Ni, along whose boundaries complex AlNi-based intermetallic compounds are located **(Fig. 1, *b*)**. The composition of the Al, V, Ti, Cr-based solid solution includes

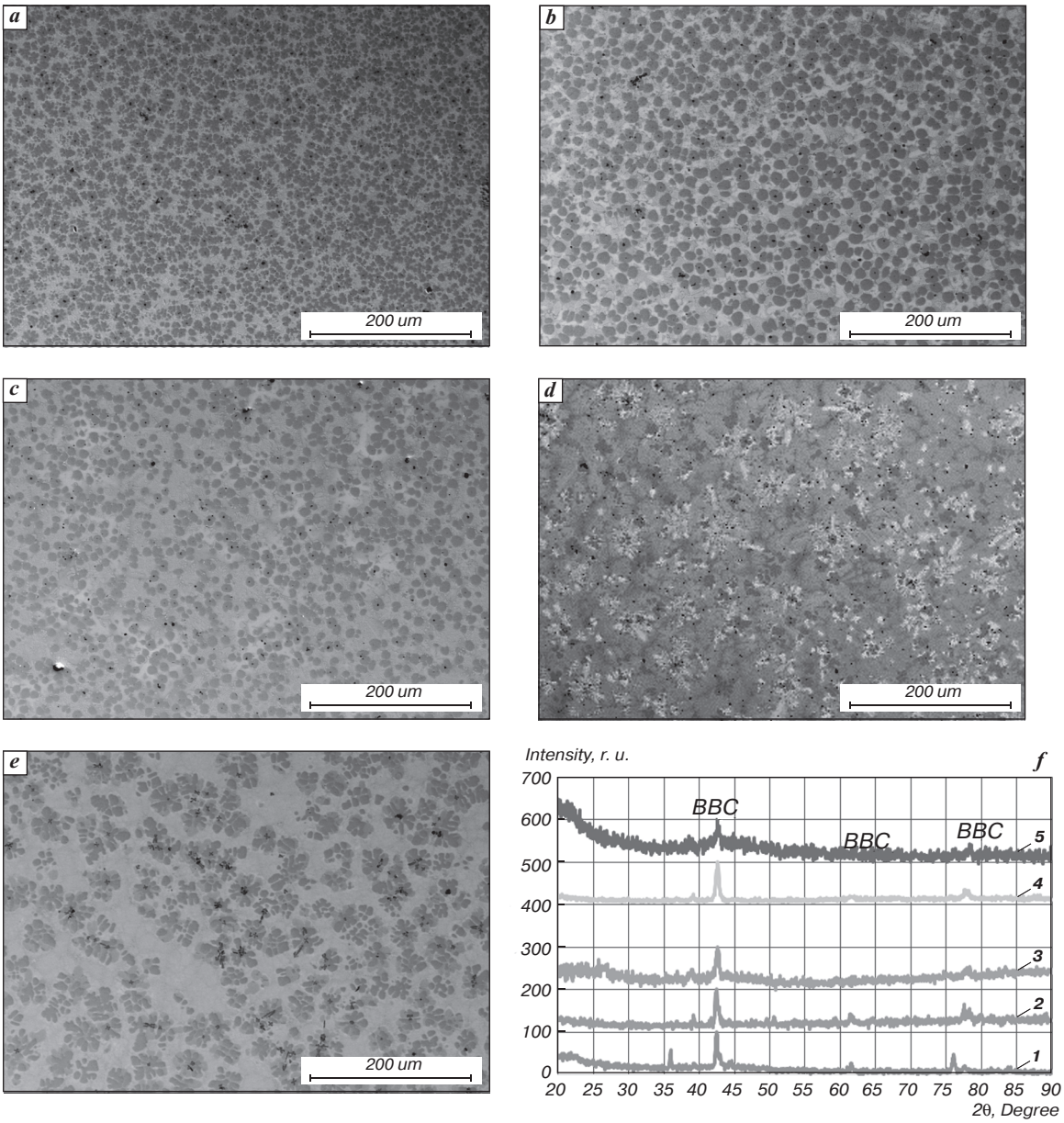

Fig. 1. Microstructure of the synthesized alloys (*1–5*) with points of micro-*X*-ray spectral analysis (*a–e*) and their corresponding *X*-ray diffraction patterns (*f*)

all alloy components except Zr. In contrast, the intermetallic inclusions contain Zr. An increase in zirconium content above 10 wt.% (Alloy 4) leads to a higher volume fraction of fine-dispersed intermetallic phases based on Zr (e.g., $ZrAl_2$, $ZrAl_3$), which, according to the literature, act as effective barriers to dislocation movement. This dispersion strengthening mechanism is the primary reason for achieving the maximum microhardness (1088 HV) and wear resistance in these coatings.

The microhardness of the coatings was measured on polished cross-sections **(Table 3)**. The microhardness values exhibit minor variations (±12%) across the coating thickness. The average values are given in **Table 3**. A notable increase in microhardness values should be noted in all parts of the coatings formed by alloys 4 and 5, where the Zr content is 4.45 and 5.5 wt.%, respectively.

Table 2
Elemental composition of the structural constituents in the anode alloys and the microhardness of the matrix grains

Structural constituents	Al	Ti	V	Cr	Ni	Zr	Microhardness of the matrix, $HV_{0.1}$
Alloy 1							
AlNi + $(Al,Ni)_3Ti_2$ + $Al_{16}Ni_7Ti_6$	43.83	23.13	4.89	6.88	16.42	4.84	
$Al_{16}Ni_7Ti_6$	50.97	16.59	4.57	5.39	18.52	3.97	
(Cr,Ti)(AlV)	33.30	8.42	27.95	27.10	3.23	–	824
Alloy 2							
AlNi + $(Al,Ni)_3Ti_2$ + $Al_{16}Ni_7Ti_6$	42.30	22.88	4.18	9.72	13.71	7.22	
(Cr,Ti)(Al,V)	31.65	8.78	23.24	33.30	3.03	–	886
Alloy 3							
AlNi + $(Al,Ni)_3Ti_2$ + $Al_{16}Ni_7Ti_6$	41.65	20.57	3.67	9.82	16.54	7.75	
(Cr,Ti)(Al,V)	28.61	7.00	21.82	39.12	3.46	–	924
Alloy 4							
AlNi + $(Al,Ni)_3Ti_2$ + $Ti_6Al_{16}Ni_7$	44.57	19.82	3.06	10.81	11.69	10.05	
(Cr,Ti)(Al,V)	45.37	7.85	13.42	29.15	3.80	–	778
Alloy 5							
AlNi + $(Al,Ni)_3Ti_2$ + $Al_{16}Ni_7Ti_6$	48.04	14.84	3.08	11.62	16.67	5.75	
(Cr,Ti)(Al,V)	35.75	8.13	13.89	39.68	2.56	35.75	840

Examination of the coating surface structure revealed the presence of individual microcracks up to 180 μm in length. The microcracks are distributed relatively uniformly over the surface, with no predominant localization established. The coating microstructure was studied on cross-sectional specimens. No significant differences were found in the microstructure of coatings produced using anode alloys 1–5. In all cases, the interface between the coating and the substrate is indistinguishable without etching (**Fig. 2**, *a*), and longitudinal microcracks are absent, indicating high coating-to-substrate adhesion. The microcracks previously detected on the coating surfaces were also observed in the cross-sectional structure and identified as transverse microcracks.

The obtained results from "ball-on-plane" abrasive wear tests demonstrate the potential of the coatings for applications involving dry friction and moderate loads. For a complete assessment of suitability in specific friction pairs (e.g., guides, shafts), further testing under lubricated conditions and cyclic loading is required, which is the subject of our ongoing research.

Fundamentally, the formation of microcracks is attributed to two primary factors: firstly, the tensile stresses generated during coating deposition by the electro-spark deposition (ESD) process, and secondly, the inherent brittleness of the anode alloy system. The regular spacing and vertical orientation of the microcracks observed in the coating cross-sections confirm the predominance of the first factor.

Table 3
Parameters and properties of the obtained coatings

Alloy No.	HV	h_p*, μm	Ψ**
1	944	68.78	2.4
2	952	50.48	3.3
3	956	31.76	1.9
4	1043	40.42	4.4
5	1088	38.82	3.9

*h_p – average coating thickness.
**Ψ – relative wear resistance indicator.

The application of ion etching and Scanning Electron Microscopy (SEM) enables the examination of the fine structure of the coating constituents **(Fig. 2, *a*)**. The structure of all coatings is characterized by columnar crystallites. Regions consisting of two distinct layers, both free from microcracks, were identified within the coating structure **(Fig. 2, *a*)**. The crystallites in these layers differ in their iron concentration. The lower layer (points 4–6) exhibits a high concentration of Fe (≈55–73 at.%).

The Fe concentration in the crystallites of the upper layer (points 1–3) does not exceed 5 at.%, which is consistent with its content in the crystallites located in regions containing microcracks **(Fig. 2, *a*, Table 4)**.

Results of the line analysis **(Fig. 2, *c*)** conducted across various crystallites traversed by a microcrack show a relatively monotonous variation in element concentrations

Table 4
Elemental composition in the coating crystallites

Analysis points	Element content at analysis points, at.%									
	C	Al	Si	Ti	V	Cr	Mn	Fe	Ni	Zr
1	8.87	33.51	–	7.22	14.49	15.83	–	3.95	14.80	1.34
2	4.53	35.01	–	8.09	15.52	16.24	–	3.15	16.00	1.45
3	8.69	33.91	–	8.38	13.45	14.82	–	5.35	13.98	1.41
4	8.21	14.63	0.39	3.02	5.34	6.15	0.35	55.97	5.37	0.56
5	10.98	12.35	0.64	2.42	4.59	5.13	0.34	58.78	4.32	0.45
6	9.92	5.83	0.60	1.51	2.68	2.96	0.49	73.16	2.54	0.32
7	3.59	–	0.80	–	–	0.58	0.51	94.52	–	–
8	3.68	–	0.64	–	–	0.39	0.74	94.56	–	–
9	4.02	–	0.60	–	–	0.34	0.75	94.28	–	–
10	3.95	–	0.65	–	–	0.22	0.81	94.36	–	–
11	4.39	–	0.91	–	–	0.22	0.66	93.82	–	–
12	4.24	–	0.67	–	–	0.19	0.69	94.21	–	–

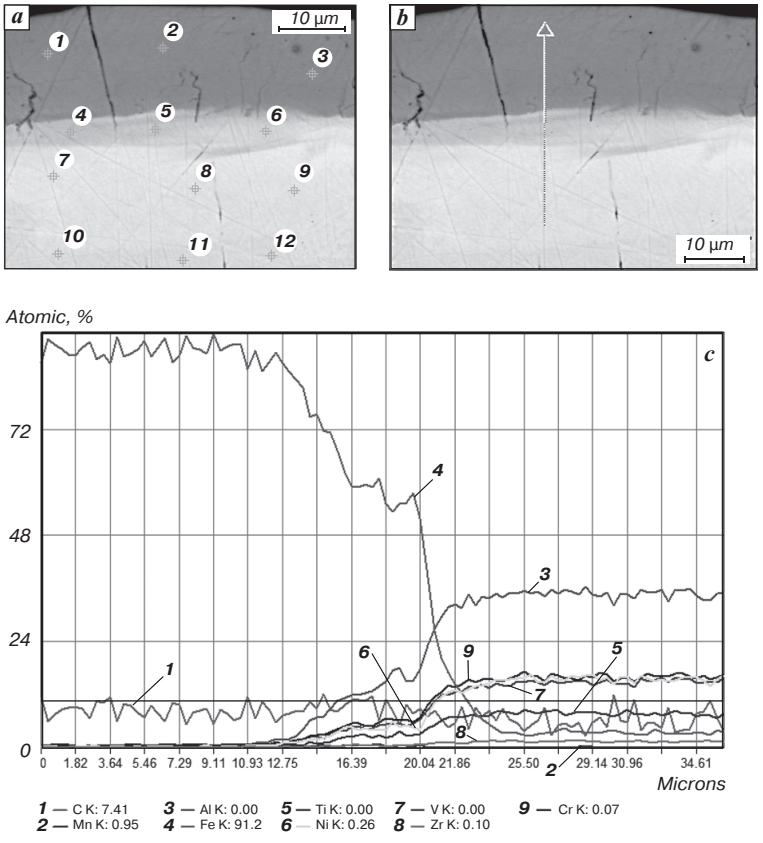

Fig. 2. Microstructure and micro-*X*-ray spectral analysis points of the coatings: *a* – coating with a microcrack; *b*, *c* – elemental distribution maps across the coating cross-section

along the length of the crystallites **(Fig. 2, *c*, Table 4)**. In other regions of the coating where microcracks are absent, the crystallites may contain an elevated iron concentration, though not exceeding 5–6 at.%.

Results of the line analysis **(Fig. 2, *c*)** conducted across various crystallites traversed by a microcrack show a relatively monotonous variation in element concentrations along the length of the crystallites **(Fig. 2, *c*, Table 4)**. In other regions of the coating where microcracks are absent, the crystallites may contain an elevated iron concentration, though not exceeding 5–6 at.%.

Given the bibliographic research data and the obtained results, it can be suggested that the abrasive wear resistance of the coatings is influenced by their brittleness. Therefore, the micro-brittleness of the coatings on the sample sections was evaluated by us using an established method [23], where an increase in the rating score indicates increased micro-brittleness of the tested material.

Conclusions

• It has been experimentally confirmed that all investigated complexly alloyed anode materials, based on solid solutions, enable the formation of coatings via the ESD process that enhance the wear resistance of Grade C45 steel. A maximum fivefold increase in wear resistance was achieved for the coating deposited from the alloy with a zirconium content of 10.4 wt.%, which is presumably attributed to dispersion strengthening by intermetallic phases.

• A direct correlation between the wear resistance and microhardness of the coatings under abrasive wear conditions has been established: the maximum values for both parameters were recorded for the same alloys (No. 4 and 5).

• The microstructure of all coatings is characterized by columnar crystallites. The presence of transverse microcracks is associated with the action of thermal tensile stresses during ESD and the inherent brittleness of the alloy materials.

A key factor suppressing microcrack formation is the development of a two-layer structure in localized coating regions. The columnar crystallites in the lower ("barrier") layer of these zones are characterized by an anomalously high concentration of iron (≥17 at.%) diffused from the substrate.

The most promising direction for further research is the targeted investigation of the formation mechanism of this defect-free, two-layer coating with an iron-rich barrier layer. Controlling this process will make it possible to minimize brittleness and further enhance the coatings' performance characteristics

Based on the conducted research, for enhancing the wear resistance of steel components under abrasive wear conditions, the use of anode alloys from the Al – Ni – Cr – Ti system with a zirconium content of approximately 10–11 wt.% (analogous to Alloys 4 and 5) is recommended. Coatings based on these alloys provide the maximum increase in microhardness (up to 1088 HV) and wear resistance (4–5 times higher than Grade C45 steel). For conditions where toughness and thermal fatigue resistance are critical, the targeted formation of a two-layer structure with an iron-saturated barrier sublayer is a promising direction

Acknowledgments

The study was conducted at the Central Collective Use Center "Applied Materials Science" of Pacific National University (PNU) with the financial support of the Ministry of Science and Higher Education of the Russian Federation (state research registration number AAAA-A20-120021490002-1).

References

1. Verbitchi V., Ciuca C., Cojocaru R. Electro-Spark Coating with Special Materials. *Nonconventional Technologies Review*. 2011. Vol. 1. pp. 57–62.

2. Zhengchuan Z., Guanjun L., Konoplyanchenko E. V., Tarelnik V. B., Zhiging G., Xin D. A Review of the Electro-Spark Deposition Technology. *Bulletin of Sumy National Agrarian University. The series: Mechanization and Automation of Production Processes*. 2021. Vol. 44, Iss. 2. pp. 45–53.

3. Barile C., Casavola C., Pappalettera G., Renna G. Advancements in Electrospark Deposition (ESD) Technique: a Short Review. *Coatings*. 2022. Vol. 12, Iss. 10. 1536.

4. Gitlevich A. E., Mikhailov V. V., Parkansky N. Ya., Revutsky V. M. Electro-Spark Alloying of Metal Surfaces. Chisinau: Shtiintsa, 1985. 198 p.

5. Vizureanu P., Perju M.-C., Dragoş C. A., Nejneru C. Advanced Electro-Spark Deposition Process on Metallic Alloys. In: *Advanced Surface Engineering Research*. 2018. pp. 45–68.

6. Zhang Y., Li L., Chang Q., Wang X.-M., Zhao Y., Zhu S., Xu A.-Y., Gao X.-W. Research Status and Prospect of Electro-Spark Deposition Technology. *Surface Technology*. 2021. Vol. 50, Iss. 1. pp. 150–161.

7. Kayali Y. Investigation of Corrosion Behavior of High Entropy Alloy Coated Ductile Iron by Electro Spark Deposition (ESD) Method. *Protection of Metals and Physical Chemistry of Surfaces*. 2025. Vol. 61, Iss. 1. pp. 146–160.

8. Wang J., Zhang M., Dai S., Zhu L. Research Progress in Electrospark Deposition Coatings on Titanium Alloy Surfaces: A Short Review. *Coatings*. 2023. Vol. 13, Iss. 8. 1473.

9. Rukanskis M. Control of Metal Surface Mechanical and Tribological Characteristics Using Cost Effective Electro-Spark Deposition. *Surface Engineering and Applied Electrochemistry*. 2019. Vol. 55, Iss. 5. pp. 607–619.

10. Penyashki T., Radev D., Kandeva M., Kostadinov G. Structural and Tribological Properties Of Wear Resistant Coatings Obtained By Electrospark Deposition. *IOP Conference Series: Materials Science and Engineering*. 2020. Vol. 724. 012015.

11. Awotunde M. A., Ayodele O. O., Adegbenjo A. O., Okoro A. M., Shongwe M. B., Olubambi P. A. NiAl Intermetallic Composites – a Review of Processing Methods, Reinforcements and Mechanical Properties. *The International Journal of Advanced Manufacturing Technology*. 2019. Vol. 104, Iss. 5. pp. 1733–1747.

12. Sampath S., Ravi V. P., Sundararajan S. An Overview on Synthesis, Processing and Applications of Nickel Aluminides: from Fundamentals to Current Prospects. *Crystals*. 2023. Vol. 13, Iss. 3. 435.

13. Yeh J. W. Recent Progress in High-Entropy Alloys. Annales de Chimie Science des Matériaux. 2006. Vol. 31, Iss. 6. pp. 633–648.

14. Zhang G., Ming K., Kang J., Huang Q., Zhang Z., Zheng X., Bi X. High Entropy Alloy as a Highly Active and Stable Electrocatalyst for Hydrogen Evolution Reaction. *Electrochimica Acta*. 2018. Vol. 279. pp. 19–23.

15. Hamdi H., Abedi H. R., Zhang Y. A Study on Outstanding High-Temperature Wear Resistance of High-Entropy Alloys. *Advanced Engineering Materials*. 2023. Vol. 25. Iss. 12. 2201915.

16. Gromov V. E., Konovalov S. V., Ivanov Yu. F., Osintsev K. A. Structure and Properties of High-Entropy Alloys. Cham, Switzerland: Springer International Publishing, 2021. 110 p.

17. Jiang N., Bian H., Song X., Wang M., Lin D., Long W., Zhong S., Jia L. Contact-Reactive Brazing of CoCrFeMnNi High-Entropy Alloy to Zr Alloys Using Cu Interlayer. *Materials Characterization*. 2023. Vol. 204. 113186.

18. Fieser D., Lan Y., Gulino A., Compagnini G., Aaron D., Mench M., Bridges D., Shortt H., Liaw P., Hu A. Synthesis and Unique Behaviors of High-Purity HEA Nanoparticles Using Femtosecond Laser Ablation. *Nanomaterials. 2*024. Vol. 14, Iss. 6. 554.

19. Wang G., Sheng G., Yu Q., Yuan X., Sun J., Jiao Y., Zhang Y. Investigation of Intergranular Penetration Behavior in Crmnfeconi HEA/304 SS Dissimilar Brazing Joints. *Intermetallics*. 2020. Vol. 126. 106940.

20. Li G., Meng X., Geng C., Wang C., Ren H., Guo X., Li S., Tao Y. Microstructure and Properties of $Al_xCr_{1-x}CoFeNi$ High-Entropy Alloys Prepared by Spark Plasma Sintering. *Materials*. 2025. Vol. 18, Iss. 4. 755.

21. Yan J., Chan K., Peng P. Fabrication of High-Entropy Alloy Coatings Using Electro-spark Deposition. *Proceedings of the 62nd Conference of Metallurgists, COM 2023*. pp. 189–200.

22. Yan J., Lopes J. G., Chan K., Scotchmer N., Oliveira J. P., Zhou Y. N., Peng P. Microstructure Characterization of AlCrFeCoNi High-Entropy Alloy Coating on Inconel 718 by Electrospark Deposition. *Materials Characterization*. 2025. Vol. 225. 115139.

23. Vinokurov E.G., Arsenkin A. M., Grigorovich K. V., Bondar' V. V. Electrodeposition and Physico-Mechanical Properties of Chromium Coatings Modified with Disperse Particles. *Protection of Metals*. 2006. Vol. 42, Iss. 3. pp. 290–294.